Journal of Hazardous Materials 196 (2011) 29–35

Contents lists available at SciVerse ScienceDirect

Journal of Hazardous Materials

journal homepage: www.elsevier.com/locate/jhazmat

# Recyclable magnetic photocatalysts of $Fe^{2+}/TiO_2$ hierarchical architecture with effective removal of Cr(VI) under UV light from water

S.C. Xu, Y.X. Zhang, S.S. Pan, H.L. Ding, G.H. Li*

*Key Laboratory of Materials Physics, Anhui Key Lab of Nanomaterials and Nanostructure, Institute of Solid State Physics, Chinese Academy of Sciences, Hefei 230031, PR China*

ARTICLE INFO

*Article history:*
Received 1 July 2011
Received in revised form 19 August 2011
Accepted 26 August 2011
Available online 2 September 2011

*Keywords:*
Magnetic
Photocatalyst
Hierarchical architecture
Fe doped $TiO_2$ tubes
Removal of Cr(VI)

ABSTRACT

We report the synthesis and photocatalytic removal of Cr(VI) from water of hierarchical micro/nanostructured $Fe^{2+}/TiO_2$ tubes. The $TiO_2$ tubes fabricated by a facile solvothermal approach show a three-level hierarchical architecture assembled from dense nanosheets nearly vertically standing on the surface of $TiO_2$ microtube. The nanosheets with a thickness of about 20 nm are composed of numerous $TiO_2$ nanocrystals with size in the range of 15–20 nm. Ferrous ions are doped into the hierarchical architecture by a reduction route. The $Fe^{2+}/TiO_2$ catalyst demonstrates an effective removal of Cr(VI) from water under UV light and the removal effectiveness reaches 99.3% at the initial Cr(VI) concentration of 10 mg $L^{-1}$. The ferrous ion in the catalyst serves not as the photo-electron trap but as an intermedium of a two-step reduction. The $TiO_2$ photoreduces the $Fe^{2+}$ ions to Fe atoms firstly, then the Fe atoms reduce the Cr(VI) to Cr(III), and the later is removed by adsorption. The hierarchical architecture of the catalyst serves as a reactor for the photocatalytic reaction of Cr(VI) ions and an effective absorbent for the removal of Cr(III) ions. The catalyst can be easily magnetically separated from the wastewater after photocatalytic reaction and recycled after acid treatment.



## 1. Introduction

Many toxic heavy metals, such as $Cr^{6+}$, $Ni^{2+}$, $Cu^{2+}$, $Cd^{2+}$ and $Pb^{2+}$, have been discharged into the environment as industrial wastes, causing serious soil and water pollution [1–4]. Among them, the Cr(VI) is more dangerous due to its highly toxic, extremely soluble and mobile, especially, it is carcinogenic and potentially mutagenic to human being [5,6]. Different techniques have been reported in literatures for the treatments of Cr(VI), such as electrocoagulation [7,8], physical and biological adsorption [9–11], ion exchange [12], membrane separation [13] and photocatalytic reduction [14,15]. The most advisable catalyst for the removal of Cr(VI) from the wastewater should be not only capable of removing the Cr(VI) thoroughly, but also easily separated from the wastewater and economically recyclable.

As an important semiconductor, $TiO_2$ has been extensively investigated for degrading organic pollutions and removing heavy metal ions from water due to its high photocatalytic activity, chemical/photocorrosion stability, low cost and safety to environment [16–19]. Since the photocatalytic reaction and adsorption easily occurs on or around material surfaces, enlarging the surface area has been proved to be an effective route to realize high performance photocatalysis. It was found that the hierarchical structures with hollow interior and porous surface exhibit an improved photocatalytic activity due to their large surface area and special micro/nanostructures, especially for those pollutants tending to be absorbed by the catalyst [20–23]. Doping with nonmetal atoms, such as N, C, S, and F, can improve the photocatalytic activity of $TiO_2$ by narrowing its forbidden band gap, upon which enhance the absorption of visible light and generation of photoelectrons [24–27]. Recently, the research activities to improve the photocatalytic activity of $TiO_2$ by doping with transition metals, such as Ag, Fe and Pt, have been flourished. The doped transition metal ions can serve as the photo-electron trap and thus facilitate the separation of electrons and holes and inhibit their recombination reactions [28–30].

In this paper, we report a strategy to synthesize $Fe^{2+}$ ions doped $TiO_2$ catalyst with a three-level hierarchical architecture, the catalyst demonstrates an effective photocatalytic removal of Cr(VI) from water under UV light. Different from previous reports, our study indicates that the ferrous ion in the catalyst serves not as the photo-electron trap but as an intermedium of a two-step reduction. We also found that the catalyst can be magnetically separated and recycled conveniently and economically.

## 2. Experimental

### 2.1. Preparation of samples

All the chemicals were of analytic grade and used without further purification. In a typical procedure, an emulsion

* Corresponding author. Tel.: +86 0551 559 1437; fax: +86 0551 559 1434.
*E-mail address:* ghli@issp.ac.cn (G.H. Li).

0304-3894/$ – see front matter © 2011 Elsevier B.V. All rights reserved.
doi:10.1016/j.jhazmat.2011.08.068

containing $TiOSO_4 \cdot 2H_2O$ (1.8013 g), glycerol (12.1 mL), and methanol (27.9 mL) was first mixed and stirred for 5 min, and then ethyl ether (8.6 mL) was added to the emulsion and stirred for another 2 min. The emulsion was then moved into a 70 mL autoclave and kept at 110 °C for 24 h, followed by natural cooling to room temperature. Finally, the precipitate was taken out from the autoclave, stirred, ultrasonic dispersed, centrifuged and washed thoroughly with alcohol, dried at 80 °C and calcined at 550 °C in flow air for 3 h.

### 2.2. Characterization

The final products were characterized by X-ray diffraction (XRD, X'Pert Pro MPD), X-ray photoelectron spectroscopy (XPS, Thermo ESCALAB 250), field emission scanning electron microscopy (FESEM, Sirion 200) and high resolution electron microscopy (HRTEM, JEM 2010). Low-temperature nitrogen sorption–desorption isotherms were measured at −195.7 °C using a gas adsorption apparatus (model: Omnisorp 100CX). Specific surface area was evaluated using the Brunauer–Emmett–Teller (BET) equation and the plot of the pore-diameter distribution was determined by using the Barrett–Joyner–Halenda (BJH) method from the desorption branch of the isotherm. The pH values were measured with Mettler Toledo pH meter (FG2/EL2). The ions concentrations were measured by ICP emission spectrometer (ICP 6000). The photocatalytic reactions were carried out under Xe lamp (XBO 500 W/H OFR VS1).

### 2.3. Reduction of Fe onto $TiO_2$ tubes

In a typical experiment, as-prepared $TiO_2$ tubes (80 mg) were immersed in a 40 mL glass bottle fill with $FeCl_2 \cdot 4H_2O$ solution (20 mL, 8 mM), ultrasonic dispersed for 1 min, and then ice bathed and stirred for 10 min. Then $NaBH_4$ (5 mL, 100 mM) was dropped in the solution in 5 min and kept stirring for 30 min. Initially, the solution turned primrose yellow from milk white, and then to silver gray. Finally, the Fe nanoparticles doped $TiO_2$ tubes were centrifuged, washed thoroughly with deionized water and dried at 70 °C. The as-prepared sample turns to dark green due to the oxidation of Fe nanoparticles. For small Fe nanoparticles, the resulted Fe oxide is mainly FeO with some $Fe_2O_3$, while for large ones the pure Fe core might still exist inside Fe oxides. The corresponding sample was named as $Fe^{2+}/TiO_2$ catalyst. For comparison, some of the $Fe^{2+}/TiO_2$ catalyst were annealed in flow air at 500 °C for 60 min to transform all the FeO and Fe to $Fe_2O_3$ (the sample has a red brown color and is named as $Fe^{3+}/TiO_2$ catalyst. Accordingly, the pure $TiO_2$ tubes are named as $TiO_2$ catalyst for simplicity).

### 2.4. Removal of Cr(VI)

A series of experiments was performed to investigate the removal capacity of each catalyst under different illumination conditions. The $TiO_2$, $Fe^{2+}/TiO_2$ and $Fe^{3+}/TiO_2$ catalysts (each 5 mg) was respectively added in nine quartz glass tubes containing 20 mL, 20 mg $L^{-1}$ $K_2Cr_2O_7$ stock solution. The suspensions were ultrasonic dispersed for 1 min, then agitated tenderly and kept in different illuminated conditions (in darkness, illuminated with visible light (>400 nm by a filter) or ultraviolet light (305–387 nm)) for 1 h and then immediately centrifuged. The catalysts were separated from the suspension and the remaining clear liquid was used for ICP measurements.

The influence of the pH value on the removal of Cr(VI) was evaluated under UV light (300 W, 1 h) on the suspension samples containing 8 mg $Fe^{2+}/TiO_2$ catalyst and 8 mL $K_2Cr_2O_7$ stock solutions (10 mg $L^{-1}$) with different pH values. After ultrasonic dispersed for 1 min, the initial pH values of suspensions were adjusted by either 5% $H_2SO_4$ or 5% NaOH solution. After photocatalytic reaction the suspensions were centrifuged, and the supernatant liquid was divided into two parts. One was examined directly by ICP and another was adjusted the pH values in the range of 7.5–8 to allow of the transformation of reduced Cr(III) to $Cr(OH)_3$ precipitation before ICP examination [31,32]. The ICP result of the first part represents the total Cr concentration remained in the supernatant liquid and that of the second part is approximately to the concentration of the remained Cr(VI) after photocatalytic reaction.

Kinetics of the photocatalytic removal of Cr(VI) was studied with $Fe^{2+}/TiO_2$ catalyst in a sample containing 25 mg $Fe^{2+}/TiO_2$ catalyst and 25 mL $K_2Cr_2O_7$ stock solutions (20 mg $L^{-1}$). After ultrasonic dispersed for 1 min, the initial pH value of the suspension was adjusted to 3.5 with 5% $H_2SO_4$ solution. The sample was illuminated with UV light (300 W) with agitating tenderly. Every 3 mL suspension was taken out from the sample after 1, 5, 30, 60, 120, 180, and 240 min time-interval illumination, and then centrifuged immediately for ICP measurement without further treatment.

The dependence of the removal capacity on Cr(VI) concentration was evaluated with $Fe^{2+}/TiO_2$ catalyst under UV illumination (300 W). Six samples contained 8 mg $Fe^{2+}/TiO_2$ catalyst and 8 mL Cr(VI) ions stock solutions with the concentration of 10, 20, 40, 80, 160 and 200 ppm were prepared, and after ultrasonic dispersed for 1 min, the initial pH value of the suspensions was adjusted to 3.5. After illuminated for 240 min, the suspensions were centrifuged immediately for ICP measurements.

The recycle ability of the catalyst was test. The $Fe^{2+}/TiO_2$ catalyst after photocatalytic reaction was soaked in 10% $HNO_3$ solution for 1 h, then washed with deionized water several times and dried at 70 °C. The reborn $Fe^{2+}/TiO_2$ catalyst was tested in fresh Cr(VI) solution under the same experimental conditions as mentioned in the section of kinetics study.

## 3. Results and discussion

### 3.1. Morphology and structure

Fig. 1 shows typical FESEM images and XRD pattern of hierarchical micro/nanostructured $TiO_2$ tubes. The hierarchical architecture is composed of numerous $TiO_2$ nanosheets on the surface of microtubes. The microtubes are about 3–10 μm in length, 800–1300 nm in diameter and 200 nm in wall thickness (Fig. 1a and b). A close-up view of Fig. 1c shows that the nanosheets nearly vertically stand on the tubular surface with random distribution. The corresponding XRD analysis (Fig. 1d) reveals that the annealed samples are composed of anatase $TiO_2$.

The three-level hierarchical structure of the $TiO_2$ tubes can be clearly seen in Fig. 2. The $TiO_2$ tube is the main body of the three-level structure, and its hollow feature can be clearly observed from the different contrasts of the dark edge and pale center (Fig. 2a). The nanosheets formed the second level (Figs. 2b) are composed of numerous $TiO_2$ nanoparticles. The nanoparticles (the third level) with the diameter of 15–20 nm have a special crystal shape of clear-cut edges and corners. HRTEM characterizations indicate that the nanoparticles are anatase $TiO_2$ single crystal (see Fig. A1). The $TiO_2$ nanocrystals are connected with each other in nearly a single layer and form a sheet-like structure of about 20 nm in thickness and 250 nm in diameter. The nanosheets stand freely on the surface of the microtube (Fig. 2a) and the nanocrystals consisting of the nanosheet are loosely connected with each other (Fig. 2b), producing numerous mesopores and nanopores in the hierarchical architecture. Such three-level hierarchical structure shows no conspicuous change after doping with Fe nanoparticles, and the Fe (or its oxides) nanoparticles with about several nanometers in diameter situate inside the $TiO_2$ matrix (mainly on the surface of $TiO_2$

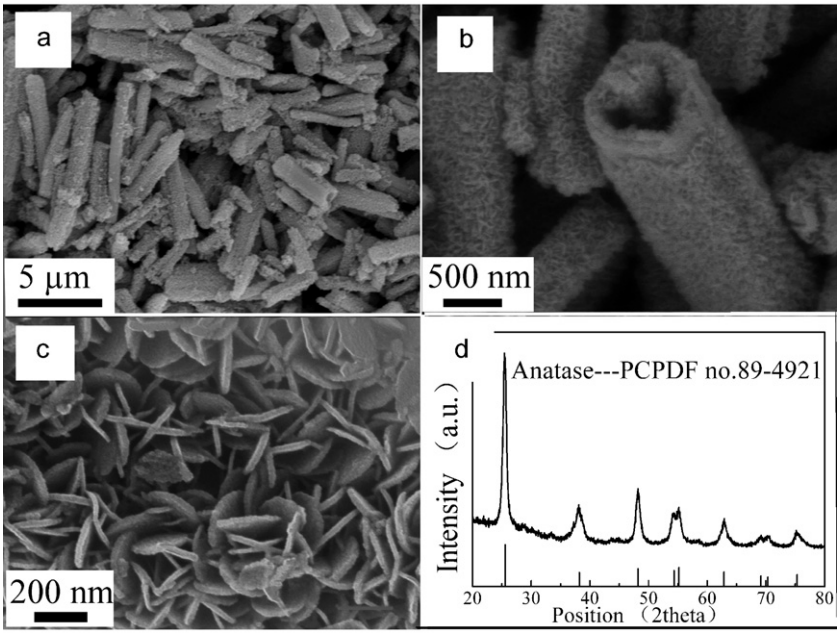


**Fig. 1.** ESEM images (a–c) and XRD pattern (d) of the $TiO_2$ tubes.

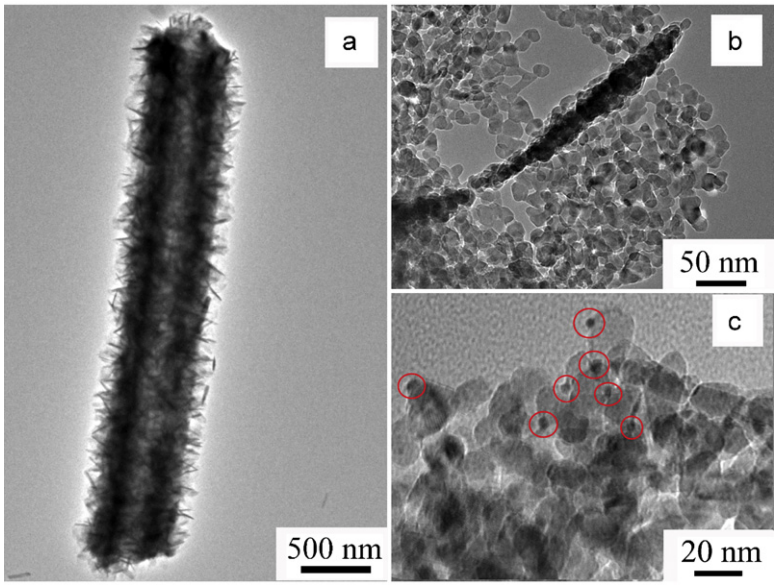


**Fig. 2.** Typical TEM image of (a) a single hierarchical micro/nanostructured $TiO_2$ tube, (b) nanosheets composed of $TiO_2$ nanocrystals, (c) Fe nanoparticles (inside the circles) doped nanosheet.

nanoparticles), as shown in Fig. 2c. It was found that the reduction step is essential in controlling the size and distribution of Fe nanoparticles inside the $TiO_2$ matrix, and the more generally direct calcination of the $TiO_2/FeCl_2$ mixture results in a large size distribution of Fe oxides.

Low-temperature nitrogen sorption–desorption isotherms measurement (Fig. 3) shows that such three-level hierarchical structured $TiO_2$ tubes have a specific surface area of about 140.3 $m^2\ g^{-1}$ (evaluated by the Brunauer–Emmett–Teller equation [33]). One can see from the pore size distribution curve (the inset in Fig. 3, calculated from desorption branch of the nitrogen isotherm by the BJH method [34]) that the nanopores have a size distribution from 5.4 to 73 nm with maximum at about 12 nm. The small pore is attributed to the interspace of the nanocrystals and the large one comes from the overlapping of the nanosheets.

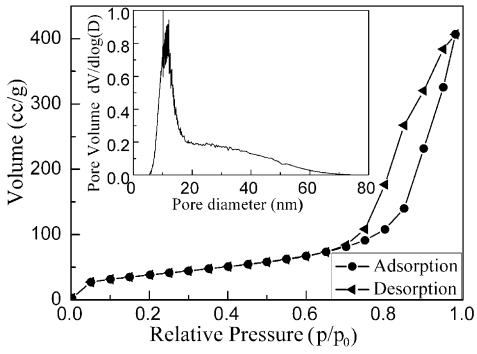


**Fig. 3.** Nitrogen sorption–desorption isotherms and pore size distribution (inset) of the $TiO_2$ tubes.

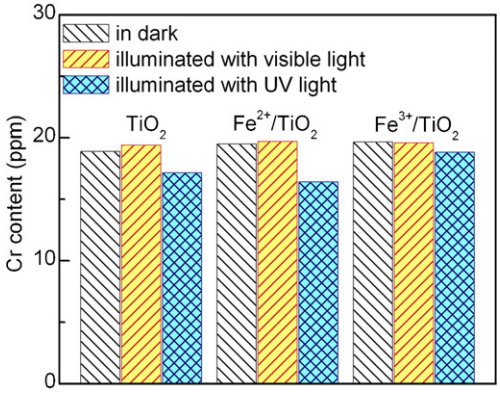


**Fig. 4.** Comparison of removal Cr(VI) capacities of $TiO_2$, $Fe^{2+}/TiO_2$ and $Fe^{3+}/TiO_2$ catalysts in dark and illuminated with visible or UV light for 1 h with the initial Cr(VI) concentration of 20 mg $L^{-1}$.

### 3.2. Mechanism of $Fe^{2+}/TiO_2$ catalyst for removal of Cr(VI) under UV light

The removal capacities of the $TiO_2$, $Fe^{2+}/TiO_2$ and $Fe^{3+}/TiO_2$ catalysts under different illumination conditions are shown in Fig. 4. Without illumination, the $TiO_2$ catalyst shows a slightly preferable removal of Cr(VI) compared with $Fe^{2+}/TiO_2$ and $Fe^{3+}/TiO_2$ catalysts, which is considered mainly due to its surface adsorption. As the $TiO_2$ catalyst is synthesized from $TiOSO_4$, the existed sulfur (as proved by the XPS analysis, see Fig. B1) will increase the surface acidity of $TiO_2$ catalyst in aqueous and make the surface more positively charged, and thus enhancing the adsorption for Cr(VI) in the form of $HCrO_4^-$, $CrO_4^{2-}$ or $Cr_2O_7^{2-}$ [35]. Under visible light illumination, the number of the photoelectron is very limited and cannot enhance the removal capacity but reduce the adsorption as the photoelectrons will neutralize some positive charges on the catalyst surface. When illuminated with UV light, the Cr(VI) will be reduced by enough photoelectrons and the removal capacity will increase accordingly. For $Fe^{2+}/TiO_2$ and $Fe^{3+}/TiO_2$ catalysts, the adsorption capacities in dark or under visible light are both lower than the $TiO_2$ catalyst because of the weakened surface acidity by Fe ions (the initial pH values of the solutions are 5.36, 6.53 and 6.05 for $TiO_2$, $Fe^{2+}/TiO_2$ and $Fe^{3+}/TiO_2$ catalysts, respectively). Interestingly, ferrous ions and ferric ions show different roles for removal of Cr(VI) under UV light. $Fe^{2+}/TiO_2$ catalyst shows an obvious improvement in removal capacity while $Fe^{3+}/TiO_2$ catalyst show a decreased removal capacity. The mechanisms for removal of Cr(VI) under UV light can be understood by the following equations:

$$TiO_2 + h\nu \rightarrow e^-_{CB} + h^+_{VB} \quad (1)$$

$$e^-_{CB} + Cr(VI) \rightarrow Cr(III)_{ads} \quad (2)$$

$$Fe^{2+} + e^-_{CB} \rightarrow Fe^0 \quad (3)$$

$$Fe^0 + Cr(VI) \rightarrow Fe^{2+}/Fe^{3+} + Cr(III)_{ads} \quad (4)$$

$$Fe^{3+} + e^-_{CB} \rightarrow Fe^{2+} \quad (5)$$

The photoelectrons generated from $TiO_2$ upon absorbing UV light can reduce Cr(VI) to Cr(III), and the Cr(III) can be removed by adsorbing on the catalyst surface according to Eqs. (1) and (2). For $Fe^{2+}/TiO_2$ catalyst, the $Fe^{2+}$ ions will be firstly reduced to $Fe^0$ atoms by the photoelectrons according to Eq. (3). The $Fe^0$ atoms have better reducibility than $Fe^{2+}$ ions and can easily reduce Cr(VI) to Cr(III) according to Eq. (4). While for $Fe^{3+}/TiO_2$ catalyst, the $Fe^{3+}$ ions will capture photoelectrons and transform to $Fe^{2+}$ ions, leading to the obvious decrease in the removal capacity according to Eq. (5). Here, the hierarchical architecture of the catalyst serves not only as a reactor for the photocatalytic reaction of Cr(VI) ions but as an effective absorbent for the removal of Cr(III) ions as well.

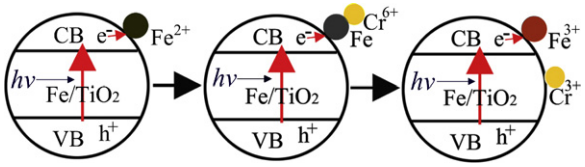


**Fig. 5.** Sketch illustration of the mechanism of photocatalytic removal of Cr(VI) for the $Fe^{2+}/TiO_2$ catalyst.

Fig. 5 illustrates the sketch mechanism of the photocatalytic removal of Cr(VI) ions in aqueous for the $Fe^{2+}/TiO_2$ catalyst. Different from the previous reports, the ferrous ions in our catalyst serve not as the photo-electron trap but as an intermedium of a two-step reduction. The $TiO_2$ photoreduces the $Fe^{2+}$ ions to Fe atoms firstly, and then the Fe atoms reduce the Cr(VI) to Cr(III). The XPS analysis further confirms our suggestion (Fig. 6). Before the photocatalytic reaction, the high-resolution spectrum shows that the binding energies of Fe 2p are at about 710.9 and 724.5 eV, corresponding respectively to Fe $2p^{3/2}$ and Fe $2p^{1/2}$, as shown in Fig. 6a, indicating that the Fe oxide is mostly composed of $Fe^{2+}$ ions. After the photocatalytic reaction, the binding energies of Fe 2p respectively shift to 713.9 and 726.5 eV, indicating that the main Fe oxide is $Fe^{3+}$ ions. The binding energies of Cr 2p adsorbed on the $Fe^{2+}/TiO_2$ catalyst are at about 577.6 and 586.8 eV (Fig. 6b), which are assigned respectively to Cr $2p^{3/2}$ and Cr $2p^{1/2}$, indicating that the adsorbed Cr ions are trivalent Cr. Because the reduction of Cr(VI) occurs mainly on the surface Fe nanoparticles, the original pure Fe core in some large Fe oxides does not affect above mentioned two-step reduction mechanism.

### 3.3. Influence of the pH value on photocatalytic activity

Fig. 7 shows the influence of the pH value on the photocatalytic activity. One can see that the $Fe^{2+}/TiO_2$ catalyst shows an excellent reducibility in the pH range from 1.85 to 6.5. At a lower pH value of 1.85, the concentration of the remained Cr(VI) is less than 0.092 ppm and the concentration of total Cr ions reaches 9.58 ppm, suggesting that most of the Cr(VI) ions are reduced to Cr(III) ions, but the adsorption capacity of the $Fe^{2+}/TiO_2$ catalyst for Cr(III) at this pH value is very low. With increasing pH value, the reducibility of $Fe^{2+}/TiO_2$ catalyst further increases (the concentration of the remained Cr(VI) is about 0.057 ppm at pH 3.5) and the adsorption capacity of Cr(III) increases dramatically (the concentration

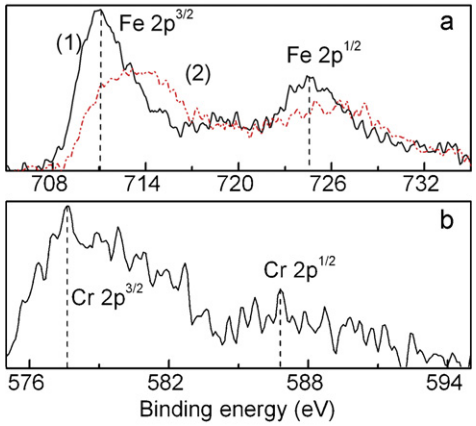


**Fig. 6.** XPS spectra of (a) Fe 2p in the $Fe^{2+}/TiO_2$ catalyst before (curve 1) and after (curve 2) photocatalytic reaction and (b) Cr 2p absorbed on the $Fe^{2+}/TiO_2$ catalyst after photocatalytic reaction.

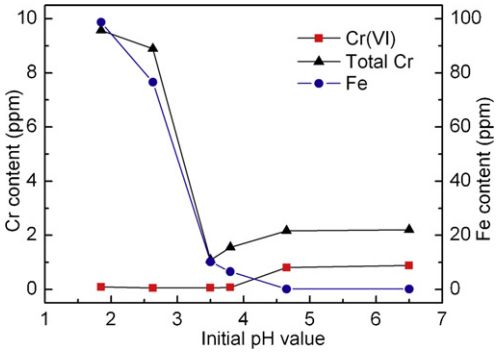


**Fig. 7.** Concentration of Cr(VI), total Cr and Fe ions remained in the photocatalytic reaction solution after 1 h illumination with 8 mg $Fe^{2+}/TiO_2$ catalyst for 8 mL Cr(VI) solution at different initial pH values (at initial concentration of 10 mg $L^{-1}$).

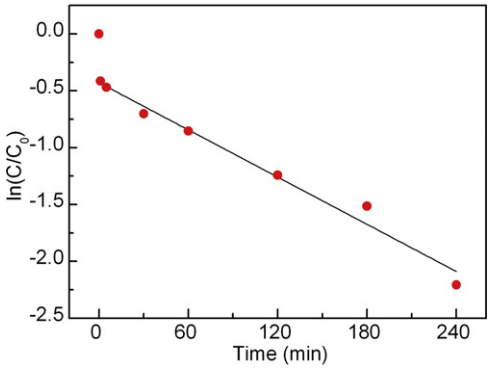


**Fig. 9.** Pseudo-first-order kinetic rate plot for removal of Cr(VI) by the $Fe^{2+}/TiO_2$ catalyst.

of total Cr ions is about 1.088 ppm at pH 3.5). As the pH value further increases from 3.8 to 6.5, the concentration of Cr(VI) and total Cr ions increases slightly. As the photocatalytic reduction depends on the $Fe^0$ atoms reduced by photoelectrons generated from $TiO_2$ under UV light, the pH value has little influence on the reducibility of the $Fe^{2+}/TiO_2$ catalyst. Whereas the adsorption of Cr(III) depends strongly on the pH value, the lower the pH value, the heavier the positively charged of the catalyst surface, and the lower the adsorption ability of Cr(III) due to the charge repel. The concentration of the Fe ions dissolved in the solution after the photocatalytic reaction is also depends on strongly on the pH value of the solution, as shown in Fig. 7. The concentration of Fe ions drops to 10.2 from 98.7 ppm as the pH value increases from 1.85 to 3.5. When the pH value is larger than 4.65 the concentration of Fe ions keeps at a nearly constant value of 0.154 ppm, indicating that the consumption of Fe is low at relative high pH value. At lower pH value, Fe atoms will apt to react with $H^+$ and dissolve into the solution, leading to the lost of the loaded Fe in the catalyst. It was found that the optimal pH values of the $Fe^{2+}/TiO_2$ catalyst for removal of Cr(VI) are in the range of 3.5–3.8.

### 3.4. Kinetics of the photocatalytic removal of Cr(VI)

Time evolution of the photocatalytic reduction of Cr(VI) by the $Fe^{2+}/TiO_2$ catalyst is characterized by optical absorption measurements, as shown in Fig. 8. At the beginning of the photocatalytic reaction, the concentration of Cr(VI) decreases rapidly and remarkably due to the high adsorption induced by the high specific surface area of the catalyst. The intensity of the absorption peaks of the Cr(VI) gradually decreases with increasing illumination time, and almost disappears after 240 min. The final concentration of the total Cr ions remained in the solution drops to 2.03 ppm from the initial 20 ppm (the inset of Fig. 8), indicating the $Fe^{2+}/TiO_2$ catalyst can effectively remove Cr(VI). The kinetics of photocatalytic reduction for Cr(VI) of the $Fe^{2+}/TiO_2$ catalyst exhibits a pseudo-first-order model as shown in Fig. 9 (except for the first minute due to the reason mentioned above). The change of $\ln(C_t/C_0)$ with respect to the reaction time has a linear form and obeys the following equation:

$$\ln\left(\frac{C_t}{C_0}\right) = A + K_{obs} \times t \tag{6}$$

where $C_0$ and $C_t$ are the concentration of Cr (VI) at initial and at different illumination times, respectively, $A$ is a experimental constant associated with the initial adsorption of the $Fe^{2+}/TiO_2$ catalyst, and $K_{obs}$ is the observed pseudo-first-order rate constant representing the photocatalytic reduction rate and can be obtained from the slope of the linear plot of $\ln(C_t/C_0)$ vs. time. In our experiments, the absolute value of $A$ and $K_{obs}$ are found to be about 0.4291 and 0.0069 $min^{-1}$, respectively.

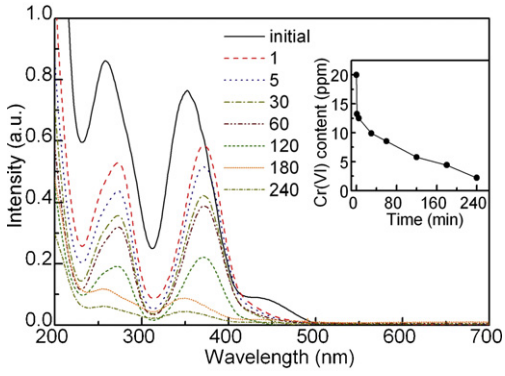


**Fig. 8.** Time dependent absorption spectra of Cr(VI) solution with initial concentration of 20 mg $L^{-1}$ after photocatalytic reaction with 25 mg $Fe^{2+}/TiO_2$ catalyst for 25 mL Cr(VI) solution. The inset shows corresponding concentrations of Cr(VI) at different reaction times.

### 3.5. Removal effectiveness and capacity on the initial concentration of Cr(VI)

The dependence of the removal effectiveness and capacity on the initial concentration of Cr(VI) was evaluated at pH 3.5 after 4 h illuminations. The removal capacity is determined by the following equation:

$$Q_e = \frac{m_r}{m} = \frac{(C_0 - C_t) \times V}{m} \tag{7}$$

where $Q_e$ is the amount of Cr(VI) ions reduced and removed by a unit mass $Fe^{2+}/TiO_2$ catalyst (expressed in mg $g^{-1}$), $m_r$ the mass of Cr(VI) ions reduced and removed (mg), $m$ the catalyst mass (g), $C_0$ the initial concentration of Cr(VI) ions (ppm or mg $L^{-1}$), $C_t$ the concentration of Cr(VI) (ppm or mg $L^{-1}$) after photocatalytic reaction and $V$ the volume of the solution from which the photocatalytic reaction occurs (L). The removal effectiveness is evaluated by the ratio of the mass of Cr(VI) ions removed over its initial mass. The results are shown in Fig. 10. The removal effectiveness is very prominent at low $C_0$ (with 99.3% for initial Cr(VI) concentration of 10 ppm and 89.0% of 20 ppm), then it gradually decreases with increasing $C_0$, and at a high $C_0$, such as at 80 ppm, the removal effectiveness becomes poor. While the removal capacity increases with increasing $C_0$, and almost has a constant value at high $C_0$. The reason for this is considered mainly due to the limited generation of $Fe^0$ atoms by the photoelectron, as our further experiment conformed that the removal effectiveness and capacity can be enhanced by extending the illumination time, for example, the removal effectiveness and capacity increases respectively from 25.78 to 34.36%

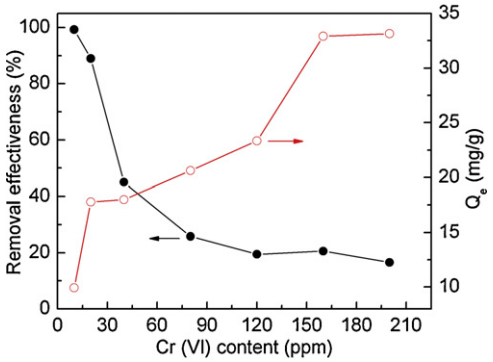


**Fig. 10.** Removal effectiveness and capacities after 4 h photocatalytic reaction at different initial Cr(VI) concentrations with 8 mg $Fe^{2+}/TiO_2$ catalyst for 8 mL Cr(VI) at initial pH value 3.5.

and 20.62 to 27.49 mg $g^{-1}$ as the illumination time prolonging from 4 to 8 h for the initial Cr(VI) concentration of 80 ppm.

### 3.6. Recycle and separation of the $Fe^{2+}/TiO_2$ catalyst

The recycle ability of the $Fe^{2+}/TiO_2$ catalyst was tested after treatment with 10% $HNO_3$. TEM characterizations show that no observable morphology change occurs after the treatment. The absorption spectra of the Cr(VI) in two cycles are shown in Fig. 11. One can see that the absorption peaks of Cr(VI) only slightly increase in the second cycle (curve 3) as compared with the first cycle (curve 2). The removal effectiveness in the second cycle is about 79.1%, which is about 89% capacity of the first cycle. The decrease in the removal effectiveness is considered mainly due to the consumption of Fe ions in the first cycle. The consumption of Fe ions during the photocatalytic reaction is shown in the inset (a) of Fig. 11, in which the consumption is negligible (below 0.01 ppm) at the first 2 h and increases to about 0.0488 ppm in the following 2 h. Such low consumption of Fe ions also indicates that the $Fe^{2+}/TiO_2$ catalyst possess favorable durability in the photocatalytic activity. Furthermore, as the $Fe^{2+}$ ions change partly to $Fe^{3+}$ ions after photocatalytic reaction, the reacted catalyst can be magnetically separated from the wastewater as shown in the inset (b) of Fig. 11. This result demonstrates that the $Fe^{2+}/TiO_2$ catalyst can be recycled conveniently and economically.

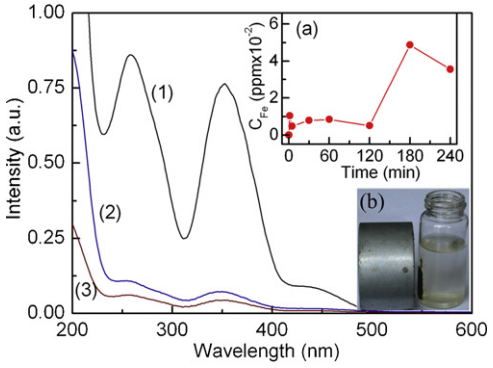


**Fig. 11.** Recyclable of the $Fe^{2+}/TiO_2$ catalyst. Cr(VI) absorption spectra of curve (1) initial, curve (2) after the first photocatalytic cycle and curve (3) after the second cycle. The inset (a) is Fe ion concentration dissolved in the solution at different photocatalytic reaction times in the first cycle and the inset (b) demonstrates the magnetically separate the catalyst from the water.

## 4. Conclusion

Three-level hierarchical micro/nanostructured $Fe^{2+}/TiO_2$ catalyst were fabricated by a facile solvothermal approach combined with a reduction route. The $Fe^{2+}/TiO_2$ catalyst shows an effective removal of Cr(VI) from water under UV light, and the removal effectiveness can reach 99.3% at the Cr(VI) initial concentration of 10 mg $L^{-1}$. The mechanism of the $Fe^{2+}/TiO_2$ catalyst for the removal of Cr(VI) ions is a two-step reduction: the $TiO_2$ catalyst photoreduces the $Fe^{2+}$ ions to Fe atoms firstly, and then the Fe atoms reduce the Cr(VI) to Cr(III). The hierarchical architecture of the catalyst serves not only as a reactor for the photocatalytic reaction of Cr(IV) ions but as an effective absorbent for the removal of Cr(III) ions as well. The catalyst can be easily magnetically separated from the wastewater after photocatalytic reaction and recycled after acid treatment conveniently and economically. The $Fe^{2+}/TiO_2$ catalyst may find potential applications as environmental benign photocatalyst for the removal of Cr(VI) from the wastewater, particularly in depth treatment of drinking water.

## Acknowledgments

The authors acknowledge the financial support from the National Natural Science Foundation of China (Grant 50802095), National Basic Research Program of China (Grant 2007CB936601) and the Foundation of President of the Hefei Institute of Physical Sciences of Chinese Academy of Sciences.

## Appendix A. Supplementary data

Supplementary data associated with this article can be found, in the online version, at doi:10.1016/j.jhazmat.2011.08.068.

## References

[1] X. Guo, G.T. Fei, H. Su, L.D. Zhang, High-performance and reproducible polyaniline nanowire/tubes for removal of Cr(VI) in aqueous solution, J. Phys. Chem. C 115 (2011) 1608–1613.
[2] M. Sprynskyy, B. Buszewski, A.P. Terzyk, J. Namiesnik, Study of the selection mechanism of heavy metal ($Pb^{2+}$, $Cu^{2+}$, $Ni^{2+}$, and $Cd^{2+}$) adsorption on clinoptilolite, J. Colloids Interface Sci. 304 (2006) 21–28.
[3] A. Sar, M. Tuzen, D. Cıtak, M. Soylak, Adsorption characteristics of Cu(II) and Pb(II) onto expanded perlite from aqueous solution, J. Hazard. Mater. 148 (2007) 387–394.
[4] K.O. Adebowale, I.E. Unuabonah, B.I. Olu-Owolabi, The effect of some operating variables on the adsorption of lead and cadmium ions on kaolinite clay, J. Hazard. Mater. B 134 (2006) 130–139.
[5] S. Rengaraj, S. Venkataraj, J. Yeon, Y. Kim, X.Z. Li, G.K.H. Pang, Preparation, characterization and application of Nd–$TiO_2$ photocatalyst for the reduction of Cr(VI) under UV light illumination, Appl. Catal. B 77 (2007) 157–165.
[6] S. Deng, R. Bai, Removal of trivalent and hexavalent chromium with aminated polyacrylonitrile fibers: performance and mechanisms, Water Res. 38 (2004) 2424–2432.
[7] I. Heidmann, W. Calmano, Removal of Zn(II), Cu(II), Ni(II), Ag(I) and Cr(VI) present in aqueous solutions by aluminium electrocoagulation, J. Hazard. Mater. 152 (2008) 934–941.
[8] P. Gao, X. Chen1, F. Shen, G. Chen, Removal of chromium (VI) from wastewater by combined electrocoagulation–electroflotation without a filter, Sep. Purif. Technol. 43 (2005) 117–123.
[9] S. Mor, K. Ravindra, N.R. Bishnoi, Adsorption of chromium from aqueous solution by activated alumina and activated charcoal, Bioresour. Technol. 98 (2007) 954–957.
[10] M.E.R. Carmona, M.A.P. da Silva, S.G.F. Leite, Biosorption of chromium using factorial experimental design, Process. Biochem. 40 (2005) 779–788.
[11] M. Kobya, Removal of Cr(VI) from aqueous solutions by adsorption onto hazelnut shell activated carbon: kinetic and equilibrium studies, Bioresour. Technol. 91 (2004) 317–321.
[12] Y. Xing, X. Chen, D. Wang, Electrically regenerated ion exchange for removal and recovery of Cr(VI) from wastewater, Environ. Sci. Technol. 41 (2007) 1439–1443.
[13] R. Guell, E. Antico, V. Salvado, C. Fontas, Efficient hollow fiber supported liquid membrane system for the removal and preconcentration of Cr(VI) at trace levels, Sep. Purif. Technol. 62 (2008) 389–393.

[14] L. Wang, N. Wang, L. Zhu, H. Yu, H. Tang, Photocatalytic reduction of Cr(VI) over different $TiO_2$ photocatalysts and the effects of dissolved organic species, J. Hazard. Mater. 152 (2008) 93–99.
[15] X. Wang, S.O. Pehkonen, A.K. Ray, Removal of aqueous Cr(VI) by a combination of photocatalytic reduction and coprecipitation, Ind. Eng. Chem. Res. 43 (2004) 1665–1672.
[16] H. Li, Z. Bian, J. Zhu, D. Zhang, G. Li, Y. Huo, H. Li, Y. Lu, Mesoporous titania spheres with tunable chamber structure and enhanced photocatalytic activity, J. Am. Chem. Soc. 129 (2007) 8406–8407.
[17] Y.X. Zhang, G.H. Li, Y.X. Jin, J. Zhang, L.D. Zhang, Hydrothermal synthesis and photoluminescence of $TiO_2$ nanowires, Chem. Phys. Lett. 365 (2002) 300–304.
[18] H. Choi, A.C. Sofranko, D.D. Dionysiou, Nanocrystalline $TiO_2$ photocatalytic membranes with a hierarchical mesoporous multilayer structure: synthesis, characterization, and multifunction, Adv. Funct. Mater. 16 (2006) 1067–1074.
[19] Y.X. Zhang, G.H. Li, Y.C. Wu, Y.Y. Luo, L.D. Zhang, The formation of mesoporous $TiO_2$ spheres via a facile chemical process, J. Phys. Chem. B 109 (2005) 5478–5481.
[20] F. Lu, W. Cai, Y. Zhang, ZnO hierarchical micro/nanoarchitectures: solvothermal synthesis and structurally enhanced photocatalytic performance, Adv. Funct. Mater. 18 (2008) 1047–1056.
[21] Y. Li, T. Sasaki, Y. Shimizu, N. Koshizaki, Hexagonal-close-packed, hierarchical amorphous $TiO_2$ nanocolumn arrays: transferability, enhanced photocatalytic activity, and superamphiphilicity without UV irradiation, J. Chem. Soc. 130 (2008) 14755–14762.
[22] Z. Liu, L. Ci, N.Y. Jin-Phillippa, M. Ruhle, Graphite-like carbon-encapsulated iron nanoparticle self-assembly into macroscopic microtube structures, J. Mater. Chem. 17 (2007) 4619–4625.
[23] X. Gong, L. Wang, W. Wen, Design and fabrication of monodisperse hollow titania microspheres from a microfluidic droplet-template, Chem. Commun. (2009) 4690–4692.
[24] J. Wang, W. Zhu, Y. Zhang, S. Liu, An efficient two-Step technique for nitrogen-doped titanium dioxide synthesizing: visible-light-induced photodecomposition of methylene blue, J. Phys. Chem. C 111 (2007) 1010–1014.
[25] K. Yang, Y. Dai, B. Huang, Understanding photocatalytic activity of S- and P-doped $TiO_2$ under visible light from first-principles, J. Phys. Chem. C 111 (2007) 18985–18994.
[26] Y. Xie, X. Zhao, Y. Li, Q. Zhao, X. Zhou, Q. Yuan, CTAB-assisted synthesis of mesoporous F–N-codoped $TiO_2$ powders with high visible-light-driven catalytic activity and adsorption capacity, J. Solid State Chem. 181 (2008) 1936–1942.
[27] W. Ren, Z. Ai, F. Jia, L. Zhang, X. Fan, Z. Zou, Low temperature preparation and visible light photocatalytic activity of mesoporous carbon-doped crystalline $TiO_2$, Appl. Catal. B 69 (2007) 138–144.
[28] Wei Zhao, Lili Feng, Rong Yang, Jie Zheng, Xingguo Li, Synthesis, characterization, and photocatalytic properties of Ag modified hollow $SiO_2/TiO_2$ hybrid microspheres, Appl. Catal. B 103 (2011) 181–189.
[29] V. Vamathevan, H. Tse, R. Amala, G. Lowb, S. McEvoy, Effects of $Fe^{3+}$ and $Ag^{+}$ ions on the photocatalytic degradation of sucrose in water, Catal. Today 68 (2001) 201–208.
[30] J. Fan, X. Liu, J. Zhang, The synthesis of $TiO_2$ and $TiO_2$-Pt and their application in the removal of Cr (VI), Environ. Technol. 32 (2011) 427–437.
[31] P.A. Kumara, S. Chakraborty, M. Ray, Removal and recovery of chromium from wastewater using short chain polyaniline synthesized on jute fiber, Chem. Eng. J. 141 (2008) 130–140.
[32] P.A. Kumara, M. Rayb, S. Chakraborty, Adsorption behaviour of trivalent chromium on amine-based polymer aniline formaldehyde condensate, Chem. Eng. J. 149 (2009) 340–347.
[33] S. Brunauer, P.H. Emmett, E. Teller, Adsorption of gases in multimolecular layers, J. Am. Chem. Soc. 60 (1938) 309–319.
[34] E.P. Barrettl, L.E. Joyner, P.P. Halenda, The determination of pore volume and area distributions in porous substances. I. computations from nitrogen isotherms, J. Am. Chem. Soc. 73 (1951) 373–380.
[35] F. Jiang, Z. Zheng, Z. Xu, S. Zheng, Z. Guo, L. Chen, Aqueous Cr(VI) photoreduction catalyzed by $TiO_2$ and sulfated $TiO_2$, J. Hazard. Mater. B 134 (2006) 94–103.